

Activity statistics of a forced elastic string in a disordered medium

Marta S de la Lama^{1,2}, Juan M López¹, José J Ramasco³
and Miguel A Rodríguez¹

¹ Instituto de Física de Cantabria (IFCA), CSIC–UC, E-39005 Santander, Spain

² Departamento de Física Moderna, Universidad de Cantabria, Avenida Los Castros, E-39005 Santander, Spain

³ Complex Systems Lagrange Laboratory, ISI Foundation, 10133 Turin, Italy
E-mail: msanchez@ifca.unican.es, lopez@ifca.unican.es, jramasco@isi.it and rodrigma@ifca.unican.es

Received 2 December 2008

Accepted 14 May 2009

Published 1 July 2009

Online at stacks.iop.org/JSTAT/2009/P07009

doi:[10.1088/1742-5468/2009/07/P07009](https://doi.org/10.1088/1742-5468/2009/07/P07009)

Abstract. We use a discrete model to study the non-equilibrium dynamics of a slowly driven elastic string in a two-dimensional disordered medium at finite temperatures. We focus on the local activity statistics to show that it can be related to global observables like the average interface velocity and the temporal correlations of the velocity fluctuations. For low temperatures the string exhibits typical creep motion and the activity statistics follows a power law, consistent with an exponential distribution of energy barriers. However, we find that the activity statistics is essentially different when the temperature is low enough, suggesting a different relaxation mechanism as $T \rightarrow 0$. We argue that this is due to the generic non-equilibrium nature of our model in the absence of thermal fluctuations.

Keywords: interfaces in random media (theory), kinetic roughening (theory), disordered systems (theory), avalanches (theory)

Contents

1. Introduction	2
2. The discrete model for elastic manifolds	4
3. Interface velocity: dynamical regimes	4
4. Activity statistics	7
5. Scaling theory	11
6. Conclusions	12
Acknowledgments	13
References	13

1. Introduction

The physics of elastic manifolds in disordered media has received much attention in the last two decades. This interest is mainly due to the relevance of the problem for understanding nonlinear collective transport in many disordered systems. Applications include those in the dynamics of charge density waves [1], vortex lines in type-II superconductors [2, 3], domain walls in magnetic [4]–[7] and ferroelectric materials [8, 9], and crack propagation [10].

The dynamics of a driven elastic string is the result of the interplay between the quenched disorder and the elastic interaction among the interface degrees of freedom. At zero temperature there is a threshold driving force f_c such that for $f < f_c$ random impurities are able to pin the interface in one of the very many static configurations (pinned phase). For $f > f_c$, however, random pinning forces are overcome by the external driving and the average position of the front moves at a finite velocity (flow phase). The system undergoes a critical depinning transition at $f = f_c$ with a diverging correlation length $\xi \sim (f - f_c)^{-\nu_{\text{dep}}}$ as $f \rightarrow f_c^+$. The critical exponent is $\nu_{\text{dep}} = 1/(2 - \zeta_{\text{dep}})$, where ζ_{dep} is the roughness exponent of the pinned interface at $f = f_c$.

In the presence of thermal fluctuations the picture outlined above changes considerably. At any finite temperature the depinning transition is washed out and a finite velocity exists for any driving force. For low temperatures and well below the zero-temperature depinning threshold, $f \ll f_c$, there is a slow creep regime where the interface dynamics can be described by thermally activated jumps of spatially correlated regions over the energy barriers separating different metastable states. In the creep regime the stationary interface velocity is finite but extremely low, which can be used to formulate a surprisingly successful scaling theory [11, 12] based on the physical properties of the system at equilibrium ($f = 0$). This approach gives the stationary creep velocity $v_\infty(f, T) \sim \exp[-(f_c/f)^\mu U_c/T]$, where U_c is a microscopic energy scale and the exponent $\mu = (d - 2 + 2\zeta_{\text{eq}})/(2 - \zeta_{\text{eq}})$ in $d + 1$ dimensions. The functional renormalization group approach has confirmed and expanded the conclusions of the scaling theory [13]–[15]. The recent introduction of algorithms that converge fast [16, 17] to reach the steady state has

allowed us to test the validity of the creep velocity with great accuracy [18]. The surprising conclusion of these numerical studies is that the theoretical values $\mu = \mu_{\text{eq}}$ and $\zeta = \zeta_{\text{eq}}$ are only attained at moderately low temperatures. In contrast, strong violation of the creep formula occurs for ultra-low temperatures [18]. The creep velocity law was found to be still valid, but the exponents μ and ζ clearly deviate from their equilibrium values as $T \rightarrow 0$.

The dynamics of the string in the moderate and low temperature regime exhibits glassy features [18]–[20]. This includes extremely slow relaxation times, toward the stationary state. While the stationary state of such systems has been the focus of many studies, the nonsteady dynamics, although experimentally relevant, has received less attention. Understanding such nonstationary physics is clearly crucial since it gives complementary information on the barriers and, for experiments, is needed to describe the many systems that are quenched in the glassy state and then have to relax (e.g., by changing the temperature rapidly). Theoretical attempts to tackle this problem have been made using mean field and renormalization group approaches [21]–[23]. However, direct application of these results (valid close to the critical dimension) to one-dimensional domain walls is difficult. Numerical studies in low dimension provide hints as regards this difficult problem, although they are also difficult since they have to deal with ultra-long timescales. Recently, Schehr and Le Doussal [23] investigated the relaxation regime for an initially flat interface by analyzing two-time correlation functions, as $f \rightarrow f_c$, showing by functional renormalization group methods that the transient dynamics displays universal behavior. This strongly suggests that some degree of universality is also present in the intermediate nonsteady regime.

In this paper we consider the non-equilibrium relaxation of the one-dimensional *forced* elastic string in random-field disorder for driving forces very far below the $T = 0$ depinning force. The dynamics in this regime is expected to be very different from the finite temperature dynamics just below the depinning threshold [19]. We carry out a novel type of study by focusing on the local activity statistics as the temperature is varied. At variance with most existing studies of the creep regime of the elastic line, the model that we consider does not allow for backward movements of the interface. This up/down asymmetry is relevant in some kinds of experimental systems, for instance in forced fluid imbibition, paper wetting, advancing cracks in solids, and flux lines in superconductors when an electric field is applied. This asymmetry could also illustrate the dynamics of an elastic string on ratchet-like potentials, which facilitate movement in a preferred direction.

Our numerical model for the elastic string is discrete, which allows us to characterize the activity properly. The lack of up/down symmetry is responsible of new phenomenology at very low temperatures, which is different from the equilibrium-like behavior typically observed in previous studies of the zero-temperature limit of the driven string.

A key quantity that we look at is the return probability, $\mathcal{P}_r(\tau)$, for the activity to be back at a particular site after a time τ . We show that this probability is directly connected with the interface velocity, the power spectrum $S(\omega) \sim 1/\omega^\alpha$ of velocity fluctuations, and the structure of avalanches of activity. Our analysis provides global dynamical information from a local observable, which may be useful in experiments. By means of scaling arguments we show that local activity statistics in the region of moderate temperatures can be interpreted as thermally activated jumps of spatially correlated regions over the energy barriers separating different metastable states. However, as temperature is decreased this

picture breaks down, since our model is a system that is genuinely out of equilibrium in the limit $T \rightarrow 0$.

2. The discrete model for elastic manifolds

Our model is inspired by a cellular automaton first proposed by Leschhorn [24] for the string at zero temperature. We study the one-dimensional case; generalization to higher dimensions is straightforward. We consider a semi-infinite square lattice, $L \times \infty$, and the string position h_i at each point i takes integer values. A random pinning force $\eta_i(h_i)$ is assigned to each lattice site. As corresponds to random-field disorder, η is an uncorrelated Gaussian variable with zero mean and unit variance. The surface height is a single-valued integer function $h_i(t)$ and the model is evolved at a fixed temperature T as follows. Starting from a flat initial state, the function

$$v_i(t) = \kappa(h_{i+1} + h_{i-1} - 2h_i) + \Delta^{1/2}\eta_i(h_i) + T^{1/2}\varepsilon_i(t) + f \quad (1)$$

is evaluated at time $t > 0$ for all sites $i = 1, \dots, L$. Site i moves forward, $h_i(t+1) \rightarrow h_i(t) + 1$, if and only if $v_i(t) > 0$; otherwise it remains pinned. Periodic boundary conditions in the substrate direction, $h_{L+1} = h_1$ and $h_0 = h_L$, are used. After evaluation of equation (1) for all i , the update is carried out in parallel for the whole front. Note that backward movements are not permitted.

Following [24], both stiffness κ and noise strength parameters are chosen to have the same order of magnitude, so the interface can become rough on length scales of the order of the lattice spacing. We fix $\kappa = 10$ and $\Delta^{1/2} = 20$. To analyze the slowly driven regime we employ a very small applied force $f \approx 5 \times 10^{-3} \times f_c(T=0)$, although other values have also been tested. The equation of motion can be rescaled and the dynamics of the system can be described in terms of the dimensionless temperature $\tilde{T} = T(\kappa/\Delta^2)^{1/3}$. Our results are typically averaged over 100–500 independent disorder realizations.

3. Interface velocity: dynamical regimes

In figure 1, we plot the average instantaneous velocity $v(t) = \langle \overline{\partial_t h} \rangle$ for different values of T . These temperatures are representative of the three different dynamical regimes that can be identified: high, low, and ultra-low temperatures. At high temperatures, the system rapidly relaxes towards a steady state where $v(t)$ becomes constant (see figure 1(a)). Lowering the temperature the relaxation time of $v(t)$ becomes longer, eventually diverging in our limited time window simulations. This leads to another regime in the range of temperatures $0.15 \lesssim \tilde{T} \lesssim 0.40$, where the instantaneous average velocity decays toward the stationary velocity $v_\infty(f, T)$ as a power law $v(t) - v_\infty \sim t^{-\theta(T)}$ as shown in figure 1(b). We find the velocity exponent to be $\theta = 0.82(4)$, $0.76(4)$, and $0.72(3)$ for $\tilde{T} = 0.20$, 0.24 and 0.28 , respectively. Finally, when T is lowered even further ($\tilde{T} \ll 0.15$) the interface velocity exhibits a change of behavior. We observe a series of plateaus separated by well defined and sudden drop-offs at certain typical times where the interface motion is rapidly slowed down (cf figure 1(c)). The time evolution of this latter regime strongly resemblances the dynamics described by Sibani [29] for several discrete glassy systems. It is important to note that this distinct ultra-low T regime is absent in the continuous model of the driven string, the so-called quenched Edwards–Wilkinson (QEW) equation [18].

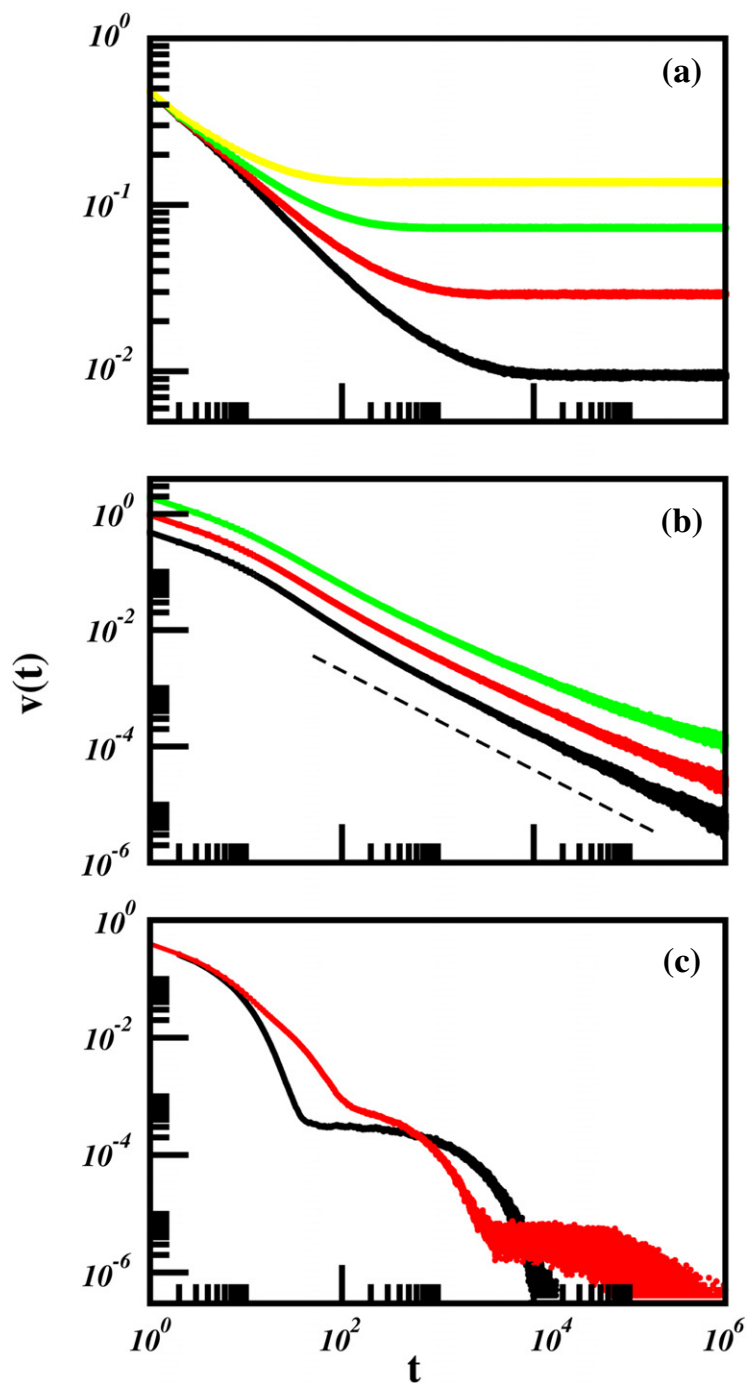


Figure 1. Interface velocity averaged over 500 runs for a system of size $L = 16\,384$. Different dynamical regimes are shown. (a) The high temperature regime for $\tilde{T} = 2$ (yellow), 1.2 (green), 0.8 (red), and 0.6 (black). (b) The low T regime for $\tilde{T} = 0.28$ (green), 0.24 (red), and 0.20 (black). Curves are vertically shifted for clarity. The dashed line has a reference slope -0.85 . (c) The ultra-low temperature regime for $\tilde{T} = 2 \times 10^{-2}$ (red) and 4×10^{-3} (black). The relative error of the velocity data is $\bar{v}/\sigma \sim 10^{-2}$ at any temperature.

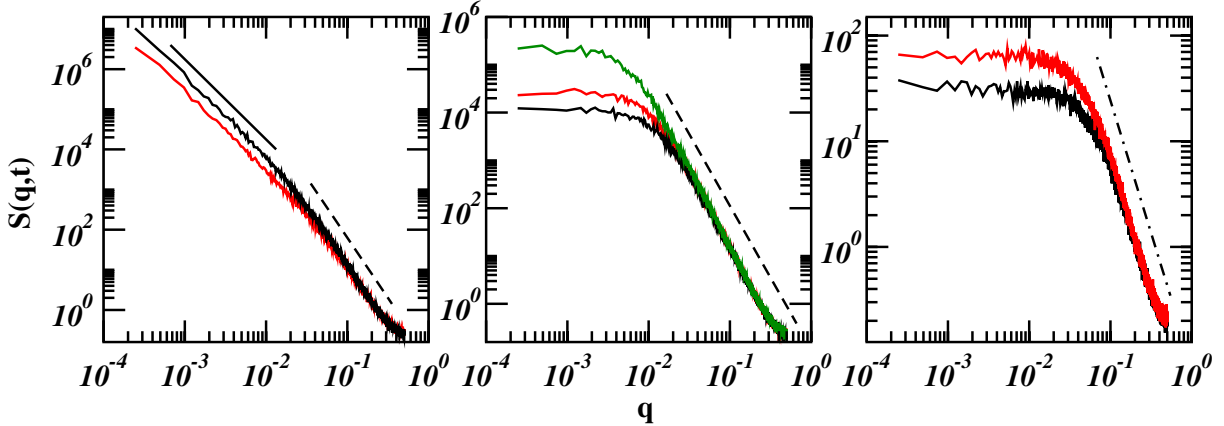


Figure 2. Structure factor for a system of size $L = 4096$ after $t = 10^6$ Monte Carlo time steps. Different dynamical regimes are shown: the high temperature regime (*left*) for $\tilde{T} = 2$ (red) and 1.2 (black); the low temperature regime (*middle*) for $\tilde{T} = 0.28$ (green), 0.24 (red) and 0.20 (black); the ultra-low temperature regime (*right*) for $\tilde{T} = 2 \times 10^{-2}$ (red) and 4×10^{-3} (black). Lines with exponent $-(2\zeta+1)$ are plotted as a guide to the eye with $\zeta_{\text{th}} = 0.5$ (*solid*), $\zeta_{\text{eq}} = 1$ (*dashed*), and $\zeta = 0.75$ (*dot-dashed*).

In order to better characterize these dynamical regimes we can look at the roughness of the interface. We employ the structure factor, that is defined in one dimension as $S(q, t) = \langle \hat{h}(q, t) \hat{h}(-q, t) \rangle$, where $\hat{h}(q, t)$ is the Fourier transform of the interface profile, and it should scale as $S(q) \sim q^{-(2\zeta+1)}$ with a roughness exponent ζ . Figure 2 shows $S(q)$ for typical temperatures within the three dynamical regimes in the long time limit.

At high temperatures we obtain a fully stationary structure factor $S(q)$ due to the fast convergence to the system toward the steady state. It scales with a roughness exponent $\zeta = \zeta_{\text{th}} \approx 0.5$ corresponding to the so-called Edwards–Wilkinson universality class [25], dominated by thermal noise. This agrees with the expected behavior of the system at high temperatures, as thermal fluctuations wash out the effect of quenched randomness and the front moves freely through the disordered medium.

In the low temperature regime, random forces are able to locally pin the interface and the relaxation time increases considerably, giving rise to a nonstationary $S(q, t)$ in the time span considered. However thermal fluctuations are able to equilibrate the line at short scales. From figure 2 we observe that at large $q > q^*(t, \tilde{T})$ the height–height correlations are well described with the equilibrium random-field exponent $\zeta = \zeta_{\text{eq}} = 1$. This seems to indicate that for moderate temperatures the quasi-equilibrium picture might hold for such scales when the interface activity is significant. These two regimes and roughness exponents, i.e. roughness $\zeta = 1/2$ and $\zeta = 1$ for high and low temperatures, respectively, are also observed in the continuous QEW model.

This picture changes in the ultra-low temperature regime, where the structure factor scales with a roughness exponent $\zeta \approx 0.75 \neq \zeta_{\text{eq}}$. Note that the range of scaling that we can obtain in this case is quite short and thus this value should be treated with some caution. In this regime the movement of the interface is so slow that the discreteness of the model and the lack of up–down symmetry of the front motion in our model become

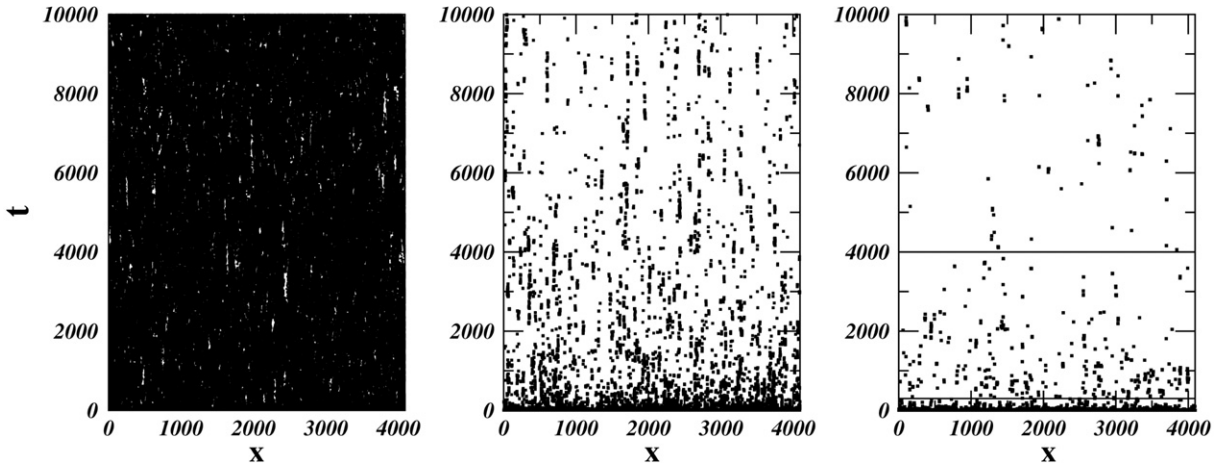


Figure 3. Activity patterns for a single realization of a system of size $L = 4096$ at three different temperatures: $\tilde{T} = 1.2$ (left), $\tilde{T} = 0.24$ (center) and $\tilde{T} = 0.04$ (right). The plots are x - t maps where the active sites are marked in black. For the lowest temperature, $\tilde{T} = 0.04$ on the right, the moments at which the system describes the characteristic drop-offs are signaled by the horizontal black lines.

relevant. Therefore, in the ultra-low T regime, the behavior of the system is not expected to be described in terms of quasi-equilibrium relaxational dynamics.

4. Activity statistics

The main advantage of the discrete model is that the activity can be directly examined. Any given site i is active at time t if $v_i(t) > 0$. The activity is therefore a binary variable taking values 1 (moving) or 0 (resting) at each site. Three of these activity maps are shown in figure 3 for the values of temperature $\tilde{T} = 0.04, 0.24$ and 1.2 , each one corresponding to a different dynamical regime. The activity patterns show a very particular shape which leads us to the use the following theoretical framework.

In order to characterize the local spatiotemporal activity we calculate the first-return time probability density, $\mathcal{P}_f(\tau)$, that stands for the probability of a site becoming active again after a period of inactivity τ . This probability describes the time intervals separating subsequent return points of activity in figure 3 at any given site and can be related to the average number of returns $n(\tau)$ in a time interval τ as follows. In the long time limit we can write $n(\tau) \sim \tau^D$, where $0 \leq D \leq 1$ is the fractal dimension of the set of return points at any given site. For $D \rightarrow 1$ activity returns become dense in time, while for $D \rightarrow 0$ returns rarely occur. In the case of a scale-invariant (fractal) activity the asymptotic ($\tau \gg 1$) distribution of first-return times is a power law, $\mathcal{P}_f(\tau) \sim \tau^{-\beta_f}$, and the scaling relation [26]

$$D = \beta_f - 1, \quad (2)$$

connecting the fractal dimension of return points with the distribution of inter-event times, can be obtained. Another important quantity is the all-times return probability $\mathcal{P}_r(\tau)$. It is defined as the conditional probability of having returning activity at time $t = \tau$ given

that the site was active at $t = 0$ (not necessarily for the first time). By definition, since $n(\tau)$ is the average number of all returns of activity in a time interval of length τ , we have $\mathcal{P}_r(\tau) = n(\tau + 1) - n(\tau)$. For a fractal activity profile this probability also shows scaling, $\mathcal{P}_r(\tau) \sim \tau^{-\beta_r}$, and one immediately obtains the relation [26]

$$\beta_f + \beta_r = 2. \quad (3)$$

Note that a fractal activity implies an infinite average return time $\langle \tau \rangle = \int_1^\infty s \mathcal{P}_f(s) ds$. Also note that, even in situations where no pure power law behavior is attained, the return probabilities are functionally related. Since the balance equation $n(\tau) = \tau - n(\tau) \int_1^\tau s \mathcal{P}_f(s) ds$ is always fulfilled, we have

$$\mathcal{P}_r(\tau) \sim \left[1 + \int_1^\tau s \mathcal{P}_f(s) ds \right]^{-1}. \quad (4)$$

The activity statistics is directly connected with the average instantaneous velocity: $v(t) \propto [n(t+1) - n(t)] \sim \mathcal{P}_r(t)$. This allows us to identify $\theta = \beta_r$ whenever the distribution $\mathcal{P}_r(t)$ is a genuine power law, i.e. $v_\infty \rightarrow 0$. In our case v_∞ is expected to be small but finite and, as we shall see below, the equality becomes only approximate, $\theta(T) \approx \beta_r(T)$ for $v_\infty \ll 1$. Finally, the Fourier transform of the velocity is $\hat{v}(\omega) \propto \int_{-\infty}^\infty \mathcal{P}_r(\tau) \exp(2\pi i \omega \tau) d\tau$ and the power spectrum $S(\omega) \propto \langle \hat{v}(\omega) \hat{v}(-\omega) \rangle \sim \omega^{-2(\beta_f-1)}$ describes the velocity correlations in the case of fractal activity. In the more general case of an exponential decay of the first-return statistics as $\mathcal{P}_f(\tau) \sim \tau^{-\beta_f} \exp(-\tau/\tau_\times)$, we have

$$S(\omega) \propto \langle \hat{v}(\omega) \hat{v}(-\omega) \rangle \sim \begin{cases} \omega^{-2(\beta_f-1)} & \text{if } \omega \gg \omega_c \\ \omega_c^{-2(\beta_f-1)} & \text{if } \omega \ll \omega_c, \end{cases} \quad (5)$$

where the cut-off frequency is $\omega_c \sim \tau_\times^{-1}$. These scaling relations link the statistics of the local waiting times to the global dynamics. In the following we describe our numerical results concerning the local activity and the global velocity of the interface in the different dynamical phases.

We plot the first-return time probability density and the return probability functions for typical temperatures within the three different dynamical regimes discussed in figure 4. At high temperatures, where the front asymptotically reaches a constant velocity and thermal fluctuations dominate the dynamics, the inter-event times show an exponential decay preceded by a power law at short times, $\mathcal{P}_f(\tau) \sim \tau^{-\beta_f} \exp(-\tau/\tau_\times)$, where β_f and τ_\times vary with temperature (cf figure 4(a)). We find that β_f varies from 1.3 to 1.5 for $\tilde{T} = 0.6$ to 2. The extent of the approximate power law regime is bounded by τ_\times and enlarges with decreasing T . This distribution implies the existence of a finite average waiting time $\langle \tau \rangle \propto \tau_\times$ for the activity to return at any given site. Since the two probability distributions are related, we can analytically calculate the asymptotic return probability, which becomes a temperature dependent constant $\mathcal{P}_r(\tau) \sim [1 + \tau_\times(T)]^{-1}$ (cf figure 4(b)) in the $\tau \gg \tau_\times$ limit. This in turn implies $\theta = 0$, and an exponential relaxation to a constant velocity. According to equation (5), the interface velocity is expected to exhibit long-range temporal correlations in this regime of temperatures, $S(\omega) \sim 1/\omega^{2D}$ for ω above a characteristic frequency $\omega_c(T) \sim 1/\tau_\times(T)$. This regime eventually crosses over to a purely thermal behavior, $S(\omega) \sim \omega^0$, at large enough frequencies (cf equation (5)). In figure 5 we plot $S(\omega)$ for several temperatures in the high temperature regime. All the spectra

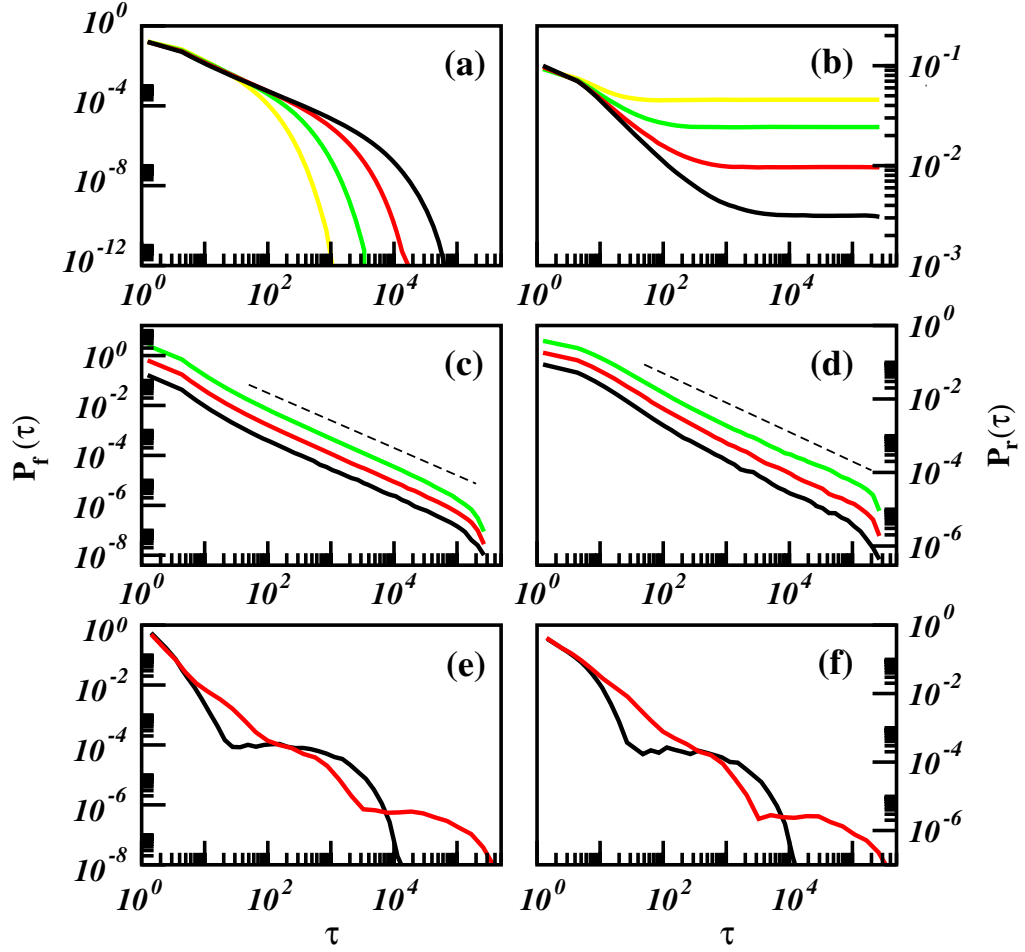


Figure 4. Activity statistics collected from 100 disorder realizations in a system of size $L = 4096$. $\mathcal{P}_f(\tau)$ is shown in the left panels and $\mathcal{P}_r(\tau)$ in the right ones. ((a), (b)) High temperature regime for $\tilde{T} = 2$ (yellow), 1.2 (green), 0.8 (red), 0.6 (black). ((c), (d)) Low temperature regime for $\tilde{T} = 0.28$ (green), 0.24 (red), 0.20 (black); curves are vertically shifted for clarity. The dashed lines with slope -1.1 in (c) and -0.8 in (d) are drawn for reference. ((e), (f)) Ultra-low temperature regime for $\tilde{T} = 2 \times 10^{-2}$ (red) and 4×10^{-3} (black).

are obtained for temporal ranges in which the signal is already stationary. The results show a good agreement with the theoretical prediction in equation (5). The existence of a $1/\omega^{2D}$ velocity spectrum with $2D \approx 0.7-1.0$ within a range of temperatures above the depinning temperature has already been observed in simulations of the QEW continuous model [20]. These long-range temporal correlations were argued to be produced by the merging of local temperature-induced avalanches of depinning events [20]. Our present analysis of activity statistics connects the $1/\omega$ noise spectrum with the recurrent activity at any given site and the avalanche distribution of active sites.

The pattern of activity is different when the temperature is decreased. For our simulation parameters, temperatures within the range $0.15 \lesssim \tilde{T} \lesssim 0.40$ (intermediate regime) lead to a first-return time distribution that exhibits a power law tail over several

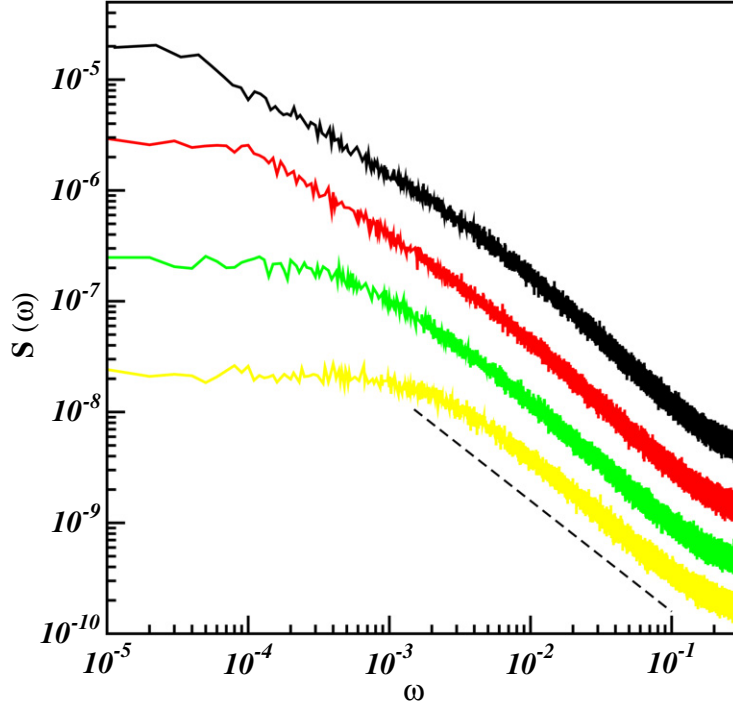


Figure 5. Spectral density $S(\omega)$ of the velocity signal for a system of size $L = 4096$ in the flowing regime at temperatures $\tilde{T} = 2$ (yellow), 1.2 (green), 0.8 (red), and 0.6 (back). Curves are vertically shifted for clarity. The dashed line has slope -1 .

decades in time $\mathcal{P}_f(\tau) \sim \tau^{-\beta_f(T)}$, with an exponent $1 < \beta_f(T) < 2$ that depends linearly on the temperature within this regime (cf figure 4(c)). This in turn implies that the return probability $\mathcal{P}_r(\tau)$ also decays as a power law (cf figure 4(d)) and the scaling relation (3) must hold. For instance, for typical temperatures within this dynamical phase we obtain $\beta_f = 1.12(5), 1.13(2), 1.15(1)$ and $\beta_r = 0.88(5), 0.86(6), 0.80(7)$, for $\tilde{T} = 0.20, 0.24, 0.28$, respectively. These values fulfil the scaling relation $\beta_f + \beta_r = 2.0(1)$. They are also in fair agreement with (but slightly different from) our direct numerical estimate of the velocity exponent θ for the same values of the temperature, as expected due to the existence of a small but finite asymptotic velocity (see the discussion after equation (4)).

The activity statistics changes even further at ultra-low temperatures, $\tilde{T} \ll 0.15$, where the local return time probabilities show rapid declines at certain characteristic times (see figures 4(e) and (f)). This behavior, similar to the one observed for other discrete glassy systems [29], is to be compared with that observed for the average velocity in figure 1(c), which is indeed expected to be the same, $v(t) \propto \mathcal{P}_r(t)$. For this ultra-low temperature the space–time activity patterns reveal that the spatial distribution of events becomes very narrowly localized around a few sites that are co-active at the same time instant. In this case the discreteness of the model becomes relevant at any scale due to the sluggish dynamics of the front. The typical creep picture [14] of coherent advances of regions L_c up to certain equilibration length $L(t)$ is not applicable here. The system stays out of equilibrium at all scales and the activity statistics is dominated by these very

local events, giving rise to the characteristic downward jumps observed in figures 1 and 4. The plateaus observed in the average velocity and the return time statistics are due to a progressive freezing of the coherent moving parts of the interface. The typical scale of this pinning region is consistent with the correlation length of the order of $\ell_x \sim 10\text{--}12$ sites, as can be seen in the structure factor plot in figure 2 (right panel). These regions move coherently at constant velocity until they become, one by one, eventually pinned by the disorder. Each time one of these regions becomes pinned there is a drop in the average velocity. The dynamics is extremely slow and the time required for a full test of the interface is far beyond our available computing time.

5. Scaling theory

A scaling theory can be developed to explain the activity statistics in our model at least for the region of moderate temperatures. For low temperatures, $T \ll U_c$, one would expect the dynamics to be governed by thermally activated jumps over the energy barriers $U(\ell)$ that have to be overcome to equilibrate the system up to the length scale ℓ , which is the mechanism leading to the characteristic creep motion. The average waiting times in these metastable configurations at a given temperature T are given by an Arrhenius law, $\langle\tau(\ell)\rangle \sim \tau_0 \exp[U(\ell)/T]$, where τ_0 is a microscopic timescale. The activity statistics can then be calculated as $\mathcal{P}_f(\tau) \sim \int dU \rho(U) \langle\tau(\ell)\rangle^{-1} e^{-\tau/\langle\tau(\ell)\rangle}$, where $\rho(U)$ is the distribution of barriers. Extreme statistics arguments [27] lead to an exponential distribution, $\rho(U) \sim \exp(-aU/U_c)$, where U_c is the minimum average energy barrier between neighboring metastable configurations at the Larkin microscopic pinning length scale L_c , and a is some dimensionless constant (see however [18]). With this choice for $\rho(U)$ one then arrives at

$$\mathcal{P}_f(\tau) \sim T \left(\frac{\tau_0}{\tau}\right)^{1+aT/U_c}, \quad (6)$$

where we can identify $\beta_f = 1 + aT/U_c$. This linear variation with T is consistent with our numerical results at low temperatures (figures 4(c) and (d)).

A distribution of first-return times as (6) would imply that the average return time $\langle\tau\rangle$ is infinite for $\beta_f < 2$, i.e. for the low temperature regime. However, as was observed by Vinokur *et al* in [27], one can assume that there exists a cut-off of the first-return time distribution arising from the elastic nature of the problem. The creep behavior is controlled by the characteristic length scale $L_{\text{opt}} = L_c (f_c/f)^{1/(2-\zeta_{\text{eq}})}$ corresponding to the optimal excitation that minimizes the free energy cost of nucleating such a perturbation [14, 27]. This typical length scale separates scales controlled by thermally activated motion ($L \ll L_{\text{opt}}$) from large scales ($L \gg L_{\text{opt}}$) that slide freely. In other words, L_{opt} gives us the upper bound above which thermally activated processes are no longer relevant. Therefore, during creep motion the average first-return time of the activity distribution is bounded from above by $\tau_{\text{max}} \sim \tau_0 \exp[U(L_{\text{opt}})/T]$, where the maximal energy barrier $U(L_{\text{opt}}) = U_c (L/L_c)^{\mu_{\text{eq}}}$. We then have $\langle\tau\rangle \sim \int_1^{\tau_{\text{max}}} s \mathcal{P}_f(s) ds$, where $\mathcal{P}_f(s)$ at temperature T is given by equation (6). The stationary velocity can then be obtained as $v_\infty \sim \langle\tau\rangle^{-1}$.

The physics behind L_{opt} (and its by-product, the maximal first-return τ_{max}) can also be invoked to explain why for low temperatures (cf figures 4(c) and (d)) $\mathcal{P}_r(\tau)$ and $\mathcal{P}_f(\tau)$

are not ‘pure’ power laws, but must exhibit a cut-off at τ_{\max} . This in turn leads to the observation (in agreement with our simulations) that the interface velocity $v(t)$ cannot decay as a power law unless the asymptotic velocity $v_{\infty}(f, T)$ is subtracted. On the other hand, in the high temperature regime the energy barrier scale U_c is expected to be renormalized by the thermal fluctuations [15, 28]. One can define a depinning temperature $T_{\text{dep}} \approx U_c(T_{\text{dep}})/a$ separating the high temperature and the low temperature regions. Now the average first-return time $\langle \tau \rangle$ is always finite and the distribution (6) becomes bounded for $T \gg T_{\text{dep}}$, independently of the value of L_{opt} .

This scaling argument allows us to understand the local activity statistics (first-return probability density and velocity) in the low and high temperature regimes and leads to conclusions consistent with our numerical results. However, the argument based on energy barriers breaks down at ultra-low temperatures due to the up/down asymmetry that causes our model to be generically out of equilibrium in the absence of thermal fluctuations ($T \rightarrow 0$). Unfortunately, at this point we do not have a theoretical understanding of the dynamics in the ultra-low temperature regime. We claim that the dynamics of our model in this regime is similar to that observed for other discrete disordered systems with glassy behavior by Sibani and co-workers [29], which is still poorly understood on general grounds.

6. Conclusions

We have introduced a discrete model to study the local activity statistics of a forced elastic interface in heterogeneous media at a finite temperature. The model presents an up/down movement asymmetry that renders the model out of equilibrium in the limit of zero temperature. The model presents three dynamic regimes, two of which are equivalent to the ones observed in the QEW continuous elastic model. Thanks to the discrete character of our model, the activity becomes a binary variable and can be precisely tracked in space and time. The model shows significant differences in activity patterns in the three regimes, those of the intermediate and low temperature regimes being especially interesting. In order to analyze these activity patterns in a quantitative way, we defined the first-time and all-times return probabilities. We find that these probabilities show a power law decay in the intermediate regime with exponents that depend on temperature. Simple scaling arguments based on an exponential distribution of energy barriers lead us to propose an expression for the probability distributions of activity in good agreement with simulations. The non-equilibrium character of the model becomes relevant as the temperature is decreased toward zero and the quasi-equilibrium arguments fail to describe the dynamics. In this ultra-low temperature regime the activity statistics is similar to that observed in certain discrete glassy systems [29].

One of our main results concerns the novel approach of studying the problem of the relaxation of the driven elastic string in terms of the local activity and avalanche statistics. We show that the activity statistics is directly connected to the interface velocity, the power spectrum $S(\omega) \sim 1/\omega^\alpha$ of velocity fluctuations, and the structure of avalanches of activity. Our analysis provides global dynamical information from a local observable. We expect this to be useful in experiments, in particular in those cases where only local probes can be used to obtain information about the position of the interface.

Acknowledgments

This work is supported by the Ministerio de Educación y Ciencia (Spain) through grants FIS2006-12253-C06-04 and CGL2007-64387/CLI. JJR was partially funded by the Progetto Lagrange of the CRT Foundation. The authors gratefully acknowledge the computer resources, technical expertise and assistance provided by the FP6 Interactive European Grid project coordinated by CSIC.

References

- [1] Grüner G, 1988 *Rev. Mod. Phys.* **60** 1129
- [2] Blatter G *et al*, 1994 *Rev. Mod. Phys.* **66** 1125
- [3] Cohen L F and Jensen H J, 1997 *Rep. Prog. Phys.* **60** 1581
- [4] Lemerle S *et al*, 1998 *Phys. Rev. Lett.* **80** 849
- [5] Repain V *et al*, 2004 *Europhys. Lett.* **68** 460
- [6] Shibauchi T *et al*, 2001 *Phys. Rev. Lett.* **87** 267201
- [7] Cayssol F *et al*, 2004 *Phys. Rev. Lett.* **92** 107202
- [8] Tybell T, Paruch P, Giamarchi T and Triscone J-M, 2002 *Phys. Rev. Lett.* **89** 097601
- [9] Paruch P, Giamarchi T and Triscone J-M, 2005 *Phys. Rev. Lett.* **94** 197601
- [10] Ponson L, Bonamy D and Bouchaud E, 2006 *Phys. Rev. Lett.* **96** 035506
- [11] Feigel'man M V, Geshkenbein V B, Larkin A I and Vinokur V M, 1989 *Phys. Rev. Lett.* **63** 2303
- [12] Nattermann T, 1990 *Phys. Rev. Lett.* **64** 2454
- [13] Chauve P, Giamarchi T and Le Doussal P, 1998 *Europhys. Lett.* **44** 110
- [14] Chauve P, Giamarchi T and Le Doussal P, 2000 *Phys. Rev. B* **62** 6241
- [15] Müller M, Gorokhov D A and Blatter G, 2001 *Phys. Rev. B* **63** 184305
- [16] Rosso A and Krauth W, 2001 *Phys. Rev. B* **65** 012202
- [17] Rosso A and Krauth W, 2001 *Phys. Rev. Lett.* **87** 187002
- [18] Kolton A B, Rosso A and Giamarchi T, 2005 *Phys. Rev. Lett.* **94** 047002
- [19] Kolton A B, Rosso A and Giamarchi T, 2006 *Phys. Rev. Lett.* **97** 057001
- [20] Ramasco J J, López J M and Rodríguez M A, 2006 *Europhys. Lett.* **76** 554
- [21] Cugliandolo L F, Kurchan J and Le Doussal P, 1996 *Phys. Rev. Lett.* **76** 2390
- [22] Balents L and Le Doussal P, 2004 *Phys. Rev. E* **69** 061107
- [23] Schehr G and Le Doussal P, 2004 *Phys. Rev. Lett.* **93** 217201
Schehr G and Le Doussal P, 2005 *Europhys. Lett.* **71** 290
- [24] Leschhorn H, 1993 *Physica A* **195** 324
- [25] Edwards S F and Wilkinson D R, 1982 *Proc. R. Soc. Lond. A* **381** 17
- [26] Maslov S, Paczuski M and Bak P, 1994 *Phys. Rev. Lett.* **73** 2162
- [27] Vinokur V M, Marchetti M C and Chen L W, 1996 *Phys. Rev. Lett.* **77** 1845
- [28] Nattermann T, Shapir Y and Vilfan I, 1990 *Phys. Rev. B* **42** 8577
- [29] Sibani P and Littlewood P B, 1993 *Phys. Rev. Lett.* **71** 1482
Sibani P and Dall J, 2003 *Europhys. Lett.* **64** 8
Sibani P and Jensen H J, 2004 *J. Stat. Mech.* **P10013**